Journal of Materials Chemistry

Cite this: *J. Mater. Chem.*, 2011, **21**, 3625

www.rsc.org/materials

PAPER

Solution-phase, dual LSPR-SERS plasmonic sensors of high sensitivity and stability based on chitosan-coated anisotropic silver nanoparticles†

Monica Potara,* Ana-Maria Gabudean and Simion Astilean*

Received 3rd October 2010, Accepted 8th December 2010
DOI: 10.1039/c0jm03329d

There is a need to design highly sensitive plasmonic sensors which impart a good biocompatibility and optical stability to detect low levels of analytes in biological media. In this study we report the formation of chitosan-coated silver nanoparticles of triangular shape in solution by synergistic action of chitosan and trisodium citrate in the presence of silver seeds and ascorbic acid. It has been revealed that these anisotropic silver nanoparticles entrapped in biopolymeric shells are particularly stable and can be successfully used as versatile plasmonic substrates for molecular sensing in solution. In particular, the binding of the probe molecule monolayer (*para*-aminothiophenol, *p*-ATP) at the surface of individual chitosan-coated silver nanoparticles was demonstrated both by localized surface plasmon resonance (LSPR) shifts and surface-enhanced Raman scattering (SERS) spectra. While the LSPR-shift assay is operational for signaling molecular binding events, the SERS allows identifying the probe molecules and elucidating its orientation on the metal surface. The proof of concept for biosensing applications and dual functionality of plasmonic platform are evaluated through the combined LSPR-SERS detection of significant biological molecules, adenine. The potential of chitosan–silver nanostructures to extend the standard approach of LSPR sensing by integrating SERS measurements and operate as dual plasmonic sensors would be very attractive for investigation of analytes in biological fluids.

Introduction

Noble-metal nanoparticles exhibit extremely interesting optical responses in interaction with light. When the incoming light couples with the oscillation frequency of the conduction electrons, a so-called localized surface plasmon resonance (LSPR) arises, which is manifested as an intense extinction band along with local field enhancement. Due to their unique optical and chemical properties, plasmonic nanoparticles have been utilized in surface-enhanced Raman spectroscopy (SERS),[1] metal-enhanced fluorescence (MEF),[2] biomedical diagnostics,[3] drug delivery,[4] antimicrobial action,[5] and HIV virus inhibition.[6]

In the present there is an extensive research effort to develop synthetic methods to generate silver nanoparticles of controllable and reproducible size and shape.[7–9] Apart from spherical shape, the nanoparticles of anisotropic shape exhibit multiple surface plasmon resonances and, therefore, they can demonstrate a better suitability for applications. For instance, triangular silver nanoplates show four plasmon resonances ranging from UV-visible to near-infrared (NIR), corresponding to different modes of plasmon excitation, and consequently, they are more versatile toward using different laser lines for getting larger Raman enhancements.[10] Also, in the case of MEF, the fluorescence of molecules localized in the vicinity of anisotropic nanoparticles is demonstrated to be higher than that for spherical particles.[11] More interestingly, truncated triangular silver nanoplates with a {111} lattice plane as the basal plane possess the strongest antibacterial action against gram-negative *Escherichia coli* compared to spherical and rod shaped nanoparticles.[12]

The synthesis of silver nanoparticles with precise particle size and shape is an important challenge, although this is only the first step towards their successful use in different applications. Besides the designed shape, the chemical and electrostatic stabilities of silver nanoparticles toward their transferability from the synthesis solution to biological fluids are crucial for many applications. Typically, nanoparticles are likely to undergo significant modifications such as aggregation and surface passivation when transferred in physiological media, which may obscure the relationship between their unique size- and shape-dependent properties and their biological and optical effects. Additionally, the prospect to attach specific biopolymers and biomolecules at the nanoparticle surface is highly desirable, especially for biosensing and therapeutic applications. Therefore there is an ongoing interest to design anisotropic nanoparticles which impart not only high stability and sensitivity but also exhibit good biocompatibility toward the biological media. The

Nanobiophotonics Center, Institute for Interdisciplinary Experimental Research in Bionanoscience and Faculty of Physics, Babes-Bolyai University, Treboniu Laurian Street 42, 400271 Cluj-Napoca, Romania. E-mail: monica.potara@phys.ubbcluj.ro; simion.astilean@phys.ubbcluj.ro

† Electronic supplementary information (ESI) available: Fig. S1 and S2. See DOI: 10.1039/c0jm03329d

right choice of the protecting agent is important because the polymer should allow the efficient adsorption of the analyte from the solution on the metal surface.[13]

Chitosan is a well-known biopolymer with excellent biocompatibility, biodegradability, and nontoxicity and successful use in nanomedicine in delivering therapeutic drugs, proteins, and genes.[14] To date, chitosan has been reported to assist the synthesis of noble-metal nanoparticles, mainly gold nanoparticles, although little attention has been paid to reveal its multiple roles from controlling the formation of anisotropic nanoparticles to conferring biocompatibility and protection from aggregation in solution.[15–17]

In this work, we employ a two-step approach to demonstrate for the first time that silver nanoparticles of triangular shape can be readily tailored from initial seeds by synergistic action between chitosan and trisodium citrate (TSC) in the presence of ascorbic acid. Furthermore, taking the advantage of the high stability of as-prepared chitosan-coated silver nanoparticles, we address one important challenge for targeting and sensing (bio)molecules in solution that is to enable two distinct and powerful sensing capabilities to operate with the same plasmonic particle.[18] Specifically, we quantified LSPR shifts due to adsorption of the single molecular layer of *para*-aminothiophenol (*p*-ATP) at the surface of chitosan-coated silver nanoparticles and, subsequently, we identified the probe molecule by SERS under three excitation laser lines from visible to near-infrared (NIR). The approach of combining LSPR with complementary molecular identification through SERS represents a promising route for multimodal chemical analysis to increase the reliability of biological detection. A similar approach has been demonstrated previously on nanostructured films deposited onto the solid substrate[19] but not in solution. This is mainly because of the inherent instability of metal nanostructures in solution, which can adversely influence the reproducibility and quantitative nature of these measurements. Recently, Kelly's group has succeeded in fabricating stabilized triangular silver nanoplates and, subsequently, demonstrated their high sensitivity as LSPR sensors for bulk refractive index (RI) measurements in solution.[20] Nevertheless, we believe that similar solution-phase nanostructures can be developed to display both bulk and surface RI sensitivities coupled with SERS capability for a more reliable molecular analysis. In view of biological applications, we tested the feasibility of chitosan-protected silver nanoplates to operate as versatile LSPR-SERS substrates for monitoring trace amounts of a relevant biological probe molecule, here adenine.

Experimental

Chemicals

Chitosan flakes (high molecular weight, >75% deacetylated), silver nitrate ($AgNO_3$), trisodium citrate ($C_6H_5Na_3O_7$) and *p*-aminothiophenol (*p*-ATP) were purchased from Aldrich. Glacial acetic acid (99.8%) was supplied by Sigma-Aldrich and was diluted to 1% aqueous solution before use. Ascorbic acid, sodium borohydride ($NaBH_4$) and glycerol were obtained from Merck. Adenine was purchased from Acros Organics. All chemicals were used without further purification. Solutions were prepared using ultrapure water with a resistivity of at least 18 MΩ cm. All other reagents employed for solution preparation were of analytical grade. All glassware used was cleaned with *aqua regia* solution ($HCl : NO_3$ 3 : 1) and then rinsed thoroughly with ultrapure water.

Seed preparation

A stock solution of silver particles called "seeds" was prepared in water by reduction reaction of silver nitrate with sodium borohydride. In a typical procedure, one volume of aqueous solution of silver nitrate (10 mL, 2.9×10^{-4} M) was mixed with an aqueous solution of TSC (10 mL, 2.5×10^{-4} M) and cooled in an ice-bath under vigorous stirring. To this mixture, an aqueous solution of sodium borohydride (0.6 mL, 0.1 M) was added dropwise which resulted in the formation of a bright yellow solution. The presence of seeds in solution was indicated by the UV-Vis extinction peak centered at 384 nm with a full width at the half maximum 41 nm (Fig. 1, dashed line). The as-prepared seed solution was stored in the dark 2–3 hours before use in order for any excess borohydride to react with water.

Anisotropic nanoparticles growth

Aqueous solutions of TSC (38.8 mM, 200 μL), ascorbic acid (0.1 M, 50 μL), chitosan (2 mg mL^{-1}, 10 mL) and seeds (200 μL) were

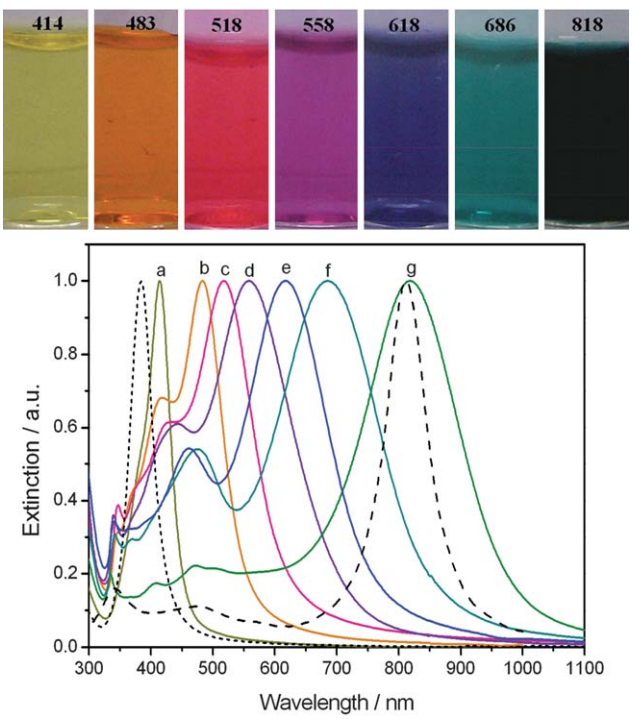

Fig. 1 Normalized UV-VIS-NIR extinction spectra and corresponding photographs of as-prepared silver colloids by increasing the TSC concentration: (a) 2.2 mM, (b) 4.8 mM, (c) 9.8 mM, (d) 19.4 mM, (e) 25 mM, (f) 30 mM and (g) 38.8 mM. The numbers on labeled vials correspond to the spectral position of the in-plane dipole resonance band. The short dashed curve represents the extinction spectrum of seeds solution. The dashed curve represents the calculated FDTD extinction spectrum of sample 1 g.

combined at 35 ± 2 °C. To this mixture, $AgNO_3$ (0.01 M, 300 μL) was added dropwise immediately under continuous magnetic stirring. The addition of silver nitrate took place during less than 1 minute. In the case of this experiment the growth of silver nanoplates finished within a total of 5 minutes under magnetic stirring. The final size and shape as well as the nanocomposites stability are strongly dependent on the specific concentration of TSC, ascorbic acid and chitosan.

Sample preparation for LSPR and SERS analysis

Water/glycerol mixtures were used to vary the *effective* (bulk) refractive index of the nanoparticle environment. The effective refractive index of water–glycerol mixture was calculated according to the Lorentz–Lorentz equation.[21] Glycerol concentrations in water were varied in eight steps as follows: 0%, 12%, 25%, 38%, 50%, 62%, 73% and 100%. For LSPR bulk sensitivity measurements, the chitosan-coated silver nanoparticles were separated from the reactive solution by centrifugation and re-suspended in the above water–glycerol mixtures of different indices of refraction. For SERS and LSPR surface sensitivity measurements, 1 mL colloidal solution of chitosan-coated silver nanostructures was incubated with 10 μL aqueous solution of *p*-ATP of different concentrations ranging from 10^{-3} M to 10^{-9} M. The final concentration of *p*-ATP in mixed samples varies from 9.9×10^{-6} M to 9.9×10^{-9} M. For LSPR and SERS measurements on adenine 800 μL colloidal solutions of chitosan-coated silver nanoparticles were incubated with a 10 μL adenine solution of 10^{-3} M. The final concentration of adenine in mixed samples was 12×10^{-6} M. The measurements were concluded after 24 hours of incubation to ensure that the system had reached the equilibrium. The minimum incubation time was monitored *via* the intensity of the SERS signal. The SERS intensity increased gradually and reached the maximum value after 24 h when the signal remained stable. However, a reasonably good SERS spectrum can be recorded about after 4 hours of incubation. We noticed that in the case of *p*-ATP molecules the incubation time for reaching a maximum signal has been shortened from 24 h to 9–10 h by magnetic stirring and for adenine to 4 h by adjusting the pH value to 5.5.

Sample characterization

The LSPR spectra were measured in a 2 mm quartz cell using a Jasco V-670 UV-VIS-NIR spectrometer with 1 nm spectral resolution. The TEM images were taken using a JEOL JEM 1010 transmission electron microscope (TEM). For TEM measurements the samples were prepared by placing a drop of colloidal dispersion onto carbon-coated copper grids and dried at room temperature. Uranyl acetate dihydrate was used as the negative contrast agent. The average size and distribution of silver nanoparticles in TEM images were determined by using Image J software for image processing.[22] SERS spectra were recorded on a confocal Raman microscope (Alpha300 from WITec) in backscattering geometry, employing 532 nm and 633 nm laser lines as the excitation source directed through a 20× objective lens with a numerical aperture (NA) of 0.4. The measurements were conducted at a power incident on the samples of 3 mW, and the integration time for spectra collection was set at 30 s per spectrum. The NIR-SERS measurements were recorded using a portable Raman spectrometer (Raman Systems R3000 CN from Ocean Optics) equipped with a 785 nm diode laser coupled to a fiber optic probe of 100 μm core diameter. The laser power was set to 100 mW and the integration time to 30 s with a single accumulation for each measurement.

Results and discussion

Anisotropic nanoparticles growth

We investigate the effect of TSC on the size and shape of silver nanoparticles by conducting the growth process in seven solutions containing various amounts of TSC, as follows: 2.2 mM, 4.8 mM, 9.8 mM, 19.4 mM, 25 mM, 30 mM and 38.8 mM. Fig. 1 shows the UV-VIS-NIR extinction spectra together with the corresponding color photographs of final solutions. The solutions display a progression of color changes from yellow to dark-green as the main LSPR peak is increasingly red-shifted. The yellow colloidal solution comes from the growth process conducted at the lowest TSC concentration (2.2 mM) and its corresponding spectrum exhibit a single extinction peak located at 414 nm, slightly asymmetric, assigned to the resonance mode of spherical silver nanoparticles.[17] At the opposite side, the colloidal solution of dark-green color comes from the growth process conducted at the highest TSC concentration (38.8 mM) and its corresponding spectrum exhibit four extinction peaks which are consistent with the plasmonic signature of triangular nanoplates, according to literature.[23] The strong band situated at 818 nm is assigned to the in-plane dipole resonance while the three less intense bands are assigned to out-of-plane dipole resonance (410–423 nm), in-plane quadrupole resonance (440–470 nm) and out-of-plane quadrupolar resonance (340 nm), respectively (see the dashed curve in Fig. 1). The other solutions prepared with intermediate TSC concentration reveal similar features. However, the corresponding bands assigned to triangular nanoplates appear spectrally shifted, the in-plane dipole resonance to blue and the out-of-plane quadrupolar resonance to red, which are dependent on nanoplate size and thickness. We notice that the overall optical extinction around 400–450 nm is higher than would be expected from pure triangular nanoplates due to the competitive response of quasi-spherical nanoparticles formed when the concentration of TSC is not optimized.

More precise information about the shape and size of nanoparticles was obtained from TEM. The TEM pictures in Fig. 2a–g show the particles formed as the TSC concentration increases, which is in agreement with the UV-VIS-NIR extinction spectra in Fig. 1a–g. For instance, Fig. 2g shows perfect triangular particles formed in the largest proportion with edge lengths from 115 to 123 nm and thickness of 11 ± 2 nm (aspect ratio 11). The analysis in Fig. S1 in the ESI† gives a high number of triangular particles. Interestingly, upon further increasing the citrate concentration above the limit of 38.8 mM the final product is dominated by large silver nanoparticles of high anisotropy like nanostars (see Fig. S2 in the ESI†). In Fig. 2h a closer view of silver nanoparticles recorded by staining contrast method clearly reveals the presence of a thin chitosan layer around the particles.

In the anisotropic growth process the chitosan itself may play an important role since it plays a role in the reduction and

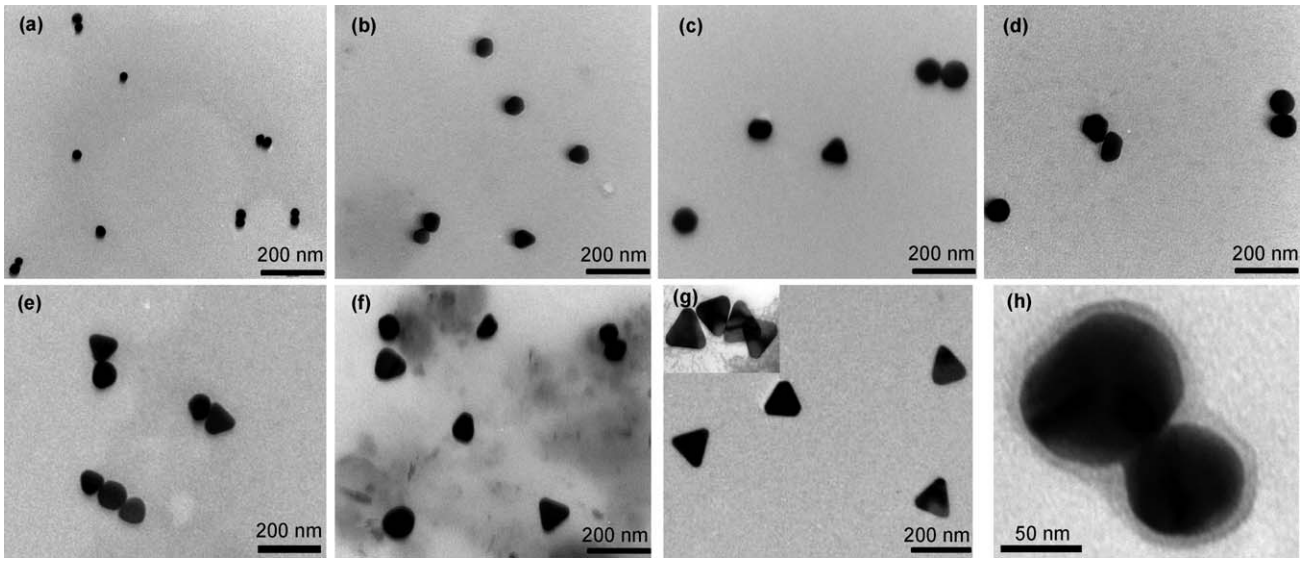

Fig. 2 TEM pictures of as-prepared silver colloids by increasing the TSC concentration: (a) 2.2 mM, (b) 4.8 mM, (c) 9.8 mM, (d) 19.4 mM, (e) 25 mM, (f) 30 mM and (g) 38.8 mM. (h) A closer view of silver nanoparticles coated by a chitosan layer.

stabilization of gold and silver nanoparticles in single-step synthesis.[16,17] To infer the role of chitosan, two comparative experiments were carried out: (a) in the absence of chitosan in solution and (b) in the presence of chitosan (2 mg mL^{-1}). Fig. 3 shows the extinction spectra recorded from the two final solutions. The analysis reveals that in the first case the spectrum (Fig. 3a) is consistent with the formation of spherical nanoparticles (dominant extinction at 423 nm) while in the second case the spectrum (Fig. 3b) is consistent with the formation of triangular particles as the quadrupole plasmon mode at 340 nm and the dipolar band at 618 nm are visible.[24] However, pure nanoplates are obtained uniquely in the presence of chitosan and high concentration TSC, clearly indicating that the two compounds act synergistically in the anisotropic growth.

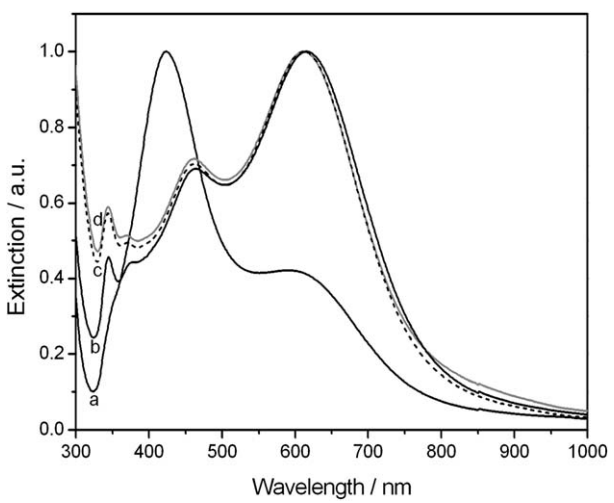

Fig. 3 Normalized UV-VIS-NIR spectra recorded from samples prepared: (a) without chitosan, (b) with 2 mg mL^{-1} chitosan, (c) sample (b) after 4 weeks of storage and (d) sample (b) after addition of 1 M NaCl.

The results above demonstrated that capping agents play a critical role for achieving triangular particles. Previous studies suggest that citrate likely induces a face-selective growth at mild temperature by binding more strongly to the silver {111} facets than {100} facets, thereby favoring the formation of silver nanoplates with {111} as the basal plane.[25] It is reasonable to admit that in our synthesis procedure preferentially interaction between sodium citrate and {111} facets could greatly reduce the growth rate along this plane and therefore promote the anisotropic growth. On the other hand, our previous studies demonstrated that chitosan may interact selectively with crystallographic planes, inhibiting the growth of these facets by lowering their surface energy and leading to the preferential orientation and growth of other planes.[16] It is conceivable that chitosan exhibits a similar behavior here by binding more strongly to {111} planes, thereby increasing the number of triangles in the final product.

In view of next step toward applications we further investigated the sample stability. We noticed that the spectrum in Fig. 3a is not stable in time. On the contrary, the spectrum in Fig. 3b did not change during many months of storage, as shown in Fig. 3c.

Next we checked the sample stability towards induced aggregation by mixing 500 μL of solution with 100 μL of a solution of NaCl (1 M), a strong aggregation agent for colloidal solution. We found again that the extinction spectrum of mixed sample remained stable (Fig. 3d). More interestingly, when the original colloidal solution was centrifuged and the solid silver–chitosan composites were re-dispersed in water or water/glycerol mixtures the initial extinction spectrum in solution was fully recovered (see details later, Fig. 4A). The affinity of amino groups in chitosan to silver surfaces could lead to adsorption of polymeric molecules on silver nanoparticles giving rise to a steric barrier that keeps the particles segregated in solution.

It comes out from the above experiments that chitosan is not only an essential component in the growth process, acting

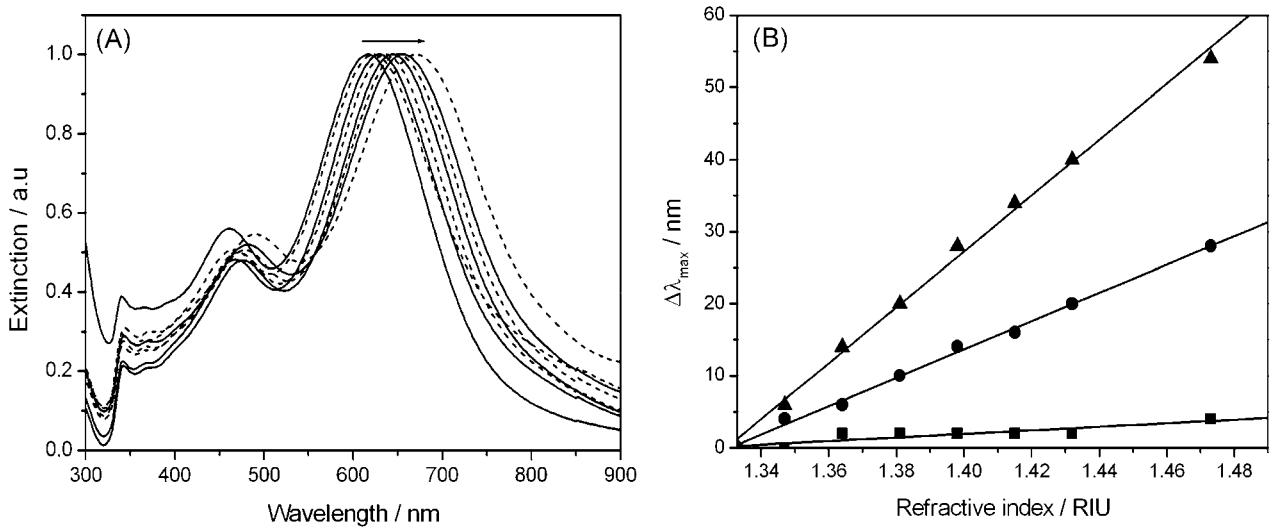

Fig. 4 (A) UV-VIS-NIR extinction spectra of silver colloid suspended in aqueous solutions of glycerol of various refractive indices, from left to right: 1.333, 1.347, 1.364, 1.381, 1.398, 1.415, 1.432, and 1.473. All spectral intensities were normalized with respect to those of the in-plane dipolar plasmonic band. (B) Plot depicting the linear dependence of the plasmonic bands position on the refractive index: (▲) in-plane dipolar plasmonic band, (●) combination of the in-plane quadrupolar band and out-of-plane dipolar mode, and (■) out-of-plane quadrupolar band.

together with TSC in shape-directing, but it also confers a very high stability and dispersibility to silver nanoplates in solution.

Dual LSPR-SERS plasmonic sensors in solution

In the following we exploit the excellent stability of chitosan-coated silver nanoparticles in combination with their optical response tunability to devise a multi-responsive plasmonic sensor in solution. Apart from particle size and shape, the LSPR peak location and intensity are sensitive to the local refractive index (RI) surrounding the nanoparticle and these features are the basis of their utility as bio–chemo-sensors. There are two kinds of changes in the environment of a nanoparticle that are of interest: (1) a bulk change, when the entire environment of the nanoparticle is modified, and (2) a local change, when only a molecular layer is adsorbed onto the nanoparticle. The latter definition has particular significance within biosensing. However, the LSPR-shift assay is not suited for molecular identification. On the contrary, the SERS is a highly specific technique to identify molecules from their unique vibrational Raman fingerprint. Here we integrate both the assays so that the probe molecules are firstly characterized with LSPR technique and then identified with the second technique that is SERS.

LSPR bulk RI sensitivity

Different water–glycerol solutions were prepared with the aim to gradually tune the RI from 1.333 (pure water) to 1.473 (pure glycerol) as described in the Experimental part.

The chitosan-coated silver nanoparticles were separated from the original solution by centrifugation and re-dispersed in the above water–glycerol solutions. Fig. 4A illustrates the normalized UV-VIS-NIR extinction spectra collected from eight water–glycerol mixtures. The similarity of extinction spectrum recorded before and after the transfer to water–glycerol mixtures clearly confirms the high stability of silver nanoparticles. Notably, the presence of chitosan around the particle did not impact negatively the exchange with the surrounding medium and liquid can come in contact with the nanoparticle surface, keeping the ability of particles to sense the modification of RI values.

The LSPR sensitivity of chitosan-coated silver nanoparticles to bulk RI of solutions was evaluated by plotting the shift of the plasmonic bands wavelength position ($\Delta\lambda_{max}$) against the refractive index (Fig. 4B). The plasmonic resonances were found to linearly red shift as the solvent refractive index was increased. The linear regression analysis yielded a bulk refractive index sensitivity of 387 nm RIU^{-1} for the in-plane dipolar plasmonic band, 196 nm RIU^{-1} for combination between the in-plane quadrupolar mode and out-of-plane dipolar mode and 25 nm RIU^{-1} for the out-of-plane quadrupolar peak, respectively. The calculated value of 387 nm RIU^{-1} for the in-plane dipolar plasmonic band at 618 nm is comparable with the sensitivity of similar triangular silver nanoplates in solution-phase value given in literature[20,26] but exceeds most of the bulk sensitivities reported in literature for various metallic nanostructures deposited onto solid substrate, as for example those of silver nanotriangles prepared by nanosphere lithography (206 nm–258 nm RIU^{-1}),[27] gold nanorods (195–288 nm RIU^{-1})[28] and spherical colloids (66.5 nm RIU^{-1}).[29] Substrate supported nanoparticles are less sensitive to a RI change than nanoparticles in a homogenous solution because some of the electromagnetic field associated with the LSPR is contained within the substrate.[27] Therefore, the plasmonic nanostructures prepared to be stable in solution represent an attractive route to achieve higher LSPR sensitivity and are promising for investigation in the natural environment of biological target molecules contained in various biological fluids.

LSPR surface sensitivity

The LSPR approach to detect the presence of biomolecular analytes was previously demonstrated for an ensemble of nanoparticles immobilized on a transparent substrate[29,30] and,

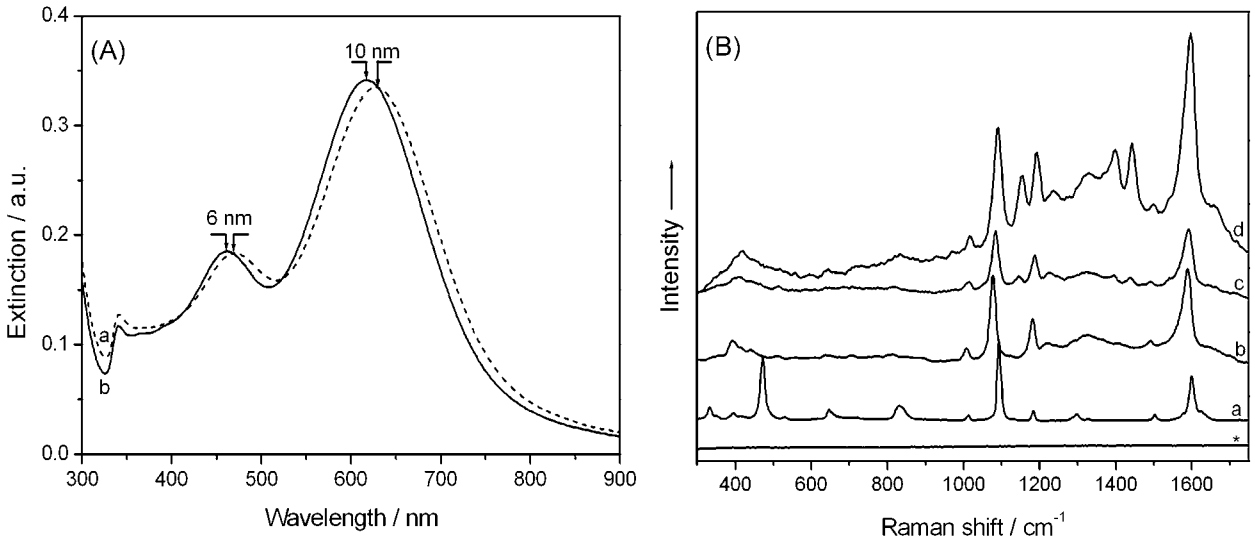

Fig. 5 (A) UV-VIS-NIR extinction spectra of silver colloid prepared with 25 mM TSC concentration: (a) after adding *p*-ATP solution and (b) before adding *p*-ATP solution. (B) The normal Raman spectrum of solid *p*-ATP (a) and SERS spectra of *p*-ATP recorded by laser excitation wavelengths 785 nm (b), 633 nm (c), and 532 nm (d). The final concentration of *p*-ATP molecules in the sample solution is 9.9×10^{-6} M. The spectrum marked by * represents the SERS spectrum from silver colloidal solution in the absence of analyte molecules.

subsequently, extended to the limit of single nanoparticles.[31,32] In our case we use anisotropic silver nanoparticles enveloped in chitosan nanoshells as a potential LSPR chemosensor in solution and *p*-ATP as the target analyte. In comparison to other molecules, thiols interact very strongly with silver surface because they may form strong covalent bonds to the surface silver atoms through back π-bonding from the sulfur bonds. Fig. 5A, part a, illustrates the extinction spectrum of *p*-ATP mixed colloidal silver nanoparticles (final *p*-ATP concentration of 9.9×10^{-6} M) recorded several hours after adding the analyte to colloidal solutions in order to achieve the maximum chemisorptions of the *p*-ATP molecules. For comparison, Fig. 5A, part b, shows the reference spectrum recorded from blank solution (without *p*-ATP). However, compared with the original spectrum of silver–chitosan nanocomposites, a decrease in the intensity of the in-plane dipolar plasmonic band with a concomitant red shift of 10 nm was observed in the presence of *p*-ATP molecules. In addition, the absorption maximum of the other bands experiences a shorter shift than that of the longitudinal band (6 nm for the out-of-plane resonance mode and 2 nm for the out-of-plane quadrupolar band). This finding is consistent with the results above which demonstrate the higher sensitivity of the in-plane dipole resonance band toward the chemical environment of these nanocomposites. The data show that chitosan acts as an excellent protective shell against aggregation and allows the analyte molecules to diffuse through its internal nanoporosities and to attach on the metal surface, which is relevant for investigation in real biological media. The presence of the analyte molecules on the silver surface leads to a change of the electrical charge on the nanoparticles surface as well as a modification of the refractive index of the medium surrounding the particles which consequently induces a decrease of the extinction band intensity and their shifts to longer wavelengths, respectively. Moreover, the shift in the maximum wavelength position of all bands demonstrates that *p*-ATP molecules immobilize not only on the edges and corners of triangles but also on its faces having a shielding effect on the silver surface. This conclusion is based on previously reported studies which demonstrate that the adsorption of analyte molecules on the preferential sites of nanoparticles surface affects only the spectral position of their corresponding plasmonic bands.[33] The ability of analytes to diffuse through the polymer matrix and immobilize to the silver nanoparticles surface while keeping their stability is an interesting feature of this system, but it is not a singular phenomenon and similar behavior was observed previously.[34,35] We have to mention that the sample demonstrates a high optical stability even after many months of storage, in contrast with the colloidal solution without chitosan which immediately aggregated after *p*-ATP addition (results not shown).

SERS sensitivity

Next we demonstrate the detection and identification of adsorbed target molecules by SERS measurements, which provide molecular specificity and higher sensitivity than LSPR measurements. High-quality SERS spectra were recorded with three laser excitation lines from visible (532 nm and 633 nm) and NIR (785 nm) as shown in Fig. 5B. The following analysis of the enhancement of specific vibrational bands clearly identifies both the presence and orientation of *p*-ATP molecules on the silver surface. The strong bands at 1093 cm^{-1} and 1596 cm^{-1} together with other two medium bands at 465 cm^{-1} and 1171 cm^{-1} are assigned to a_1 vibration modes of *p*-ATP, namely C–S stretching vibration, C–C stretching mode, C–C–C bending vibration and C–H bending mode, according to literature.[36,37] The strong enhancement of the C–S stretching vibration and the lack of a S–H stretching mode at 2558 cm^{-1} clearly suggest the rupture of S–H bond and the attachment of *p*-ATP to the silver surface through its sulfur atom. A careful analysis reveals also differences between the spectra recorded with different laser lines, as evidenced by the SERS bands observed at 1148, 1393, and 1437 cm^{-1} in the case of 532 nm laser line excitation. The assignment

of these bands is still in debate in literature, being interpreted either in terms of a metal to *p*-ATP molecule charge transfer or due to the formation of an aromatic azo-compound by photocatalytic dimerization *p*-ATP.[38,39] It is worth mentioning that the SERS enhancement is highly dependent on the excitation line (Fig. 5B). At the first sight the lower intensity of the SERS spectrum recorded with 633 nm excitation wavelengths could be surprising as the surface plasmon resonance condition seems to be better satisfied by using the 633 nm laser line (see Fig. 5A). However, similar experimental results reported in literature have demonstrated that the SERS enhancement was greater using an excitation line at a wavelength longer than that of LSPR of individual particles.[40,41]

We mention that no specific Raman signal was detected from the enveloping chitosan shell which is useful to avoid any interference with the SERS signal generated from the adsorbed molecules (see spectrum marked by * in Fig. 5B). However, the presence of the chitosan shell around the silver particles can be clearly identified by staining contrast method in TEM picture (Fig. 2h). An interesting feature is that no SERS signal appears from the polymer. Similar behavior has been previously reported in literature for other polymers used to stabilize metal nanoparticles employed as SERS-active tags or biocompatible SERS substrates.[42,43]

In view of biological applications, we tested the feasibility of chitosan-protected silver nanoplates to operate as SERS substrates in NIR with excitation at 785 nm diode laser line from a portable Raman spectrometer. We selected the 785 nm excitation due to the fact that biological tissues show minimal NIR radiation absorption and therefore this laser is more suitable for *in vivo* applications. Fig. 6 shows good-quality NIR-SERS spectra of *p*-ATP molecules in solution at concentrations ranging from 10^{-7} M to 10^{-9} M which approach the physiological concentration of many analytes in biological fluids.[18] Notably, the SERS spectra were preserved after transferring the *p*-ATP incubated nanoparticles from the initial solution to water–glycerol solution (see Fig. 6d) and even after many months of storage.

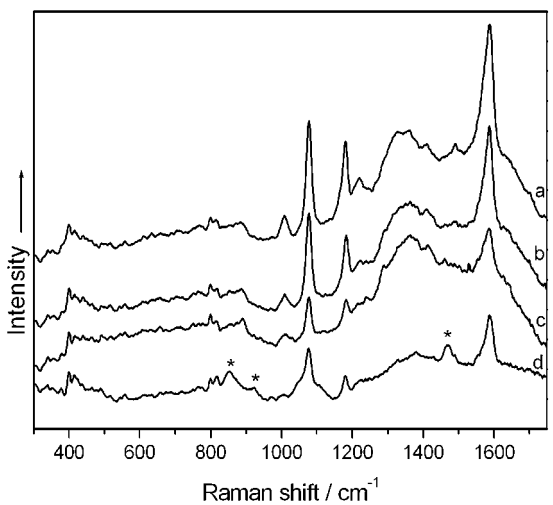

Fig. 6 The NIR-SERS spectra of different concentrations of *p*-ATP molecules in the original colloidal solution: (a) 9.9×10^{-7} M, (b) 9.9×10^{-8} M, and (c) 9.9×10^{-9} M. (d) The NIR-SERS spectrum of 9.9×10^{-6} M *p*-ATP after transferring the chitosan-coated nanoparticles from the original solution to 25% water–glycerol solution. The observation of both SERS from *p*-ATP and normal Raman peaks of glycerol (marked by *) in the recorded spectrum provides a clear evidence of the successful transfer and strong attachment of *p*-ATP *via* the thiol moiety to the surface.

Since the SERS signal shows a wavelength dependent intensity the detection limit should also vary, depending on the laser excitation line. The possibility to tune the LSPR of as-prepared colloids in a wide spectral range (from visible to NIR) provides the opportunity to select the sample with the most appropriate response to a specific requirement.

Proof of concept for biosensing applications

The ability to detect specific individual DNA bases within a sequenced genome is important for monitoring gene expression. Therefore we decided to test the performance of our approach with adenine as the analyte molecule. Adenine binding to the chitosan-coated nanoparticles is clearly demonstrated by the shift of LSPR bands in Fig. 7A.

Moreover, the identification of the adsorbed molecule can be undoubtedly supported by the analysis of SERS fingerprint recorded with three different lasers in Fig. 7B. The typical and most prominent bands at 737 and 1331 cm^{-1} observed in the SERS spectrum (Fig. 7B, parts b, c, and d) correspond to those at 722 cm^{-1} (ring breath whole molecule) and 1333 cm^{-1} (str C5–N7, N1–C2, bend C2–H, C8–H) in the ordinary Raman spectrum of adenine (Fig. 7A, part a).[44]

The preferential enhancement of the Raman bands located at 325 (bend C6–NH_2), 565 (wag C2–H, N9–H, tors NH_2), 1025 (rock NH_2), 1469 (str C2–N3, N1–C6, bend C2–H, sciss NH_2) and 1575 cm^{-1} (sciss NH_2) ascribed to the amino group vibrations relative to those of N1, N3, N9 motions around 1123 (str C8–N9, bend N9–H, C8–H), 1254 (bend C8–H, N9–H, str N7–C8) and 1606 cm^{-1} (str N3–C4, N1–C6, C5–N7, N7–C8, bend N9–H) indicates that the interaction with the silver surface takes place *via* amino groups.[45]

Based on the above experiment we anticipate that such plasmonic substrates can find useful applications in various biological environments, especially to capture and identify metabolites, pharmaceutical products or other chemicals in body fluids.

FDTD numerical simulations

To understand the source of electromagnetic enhancement in our SERS measurements, a theoretical simulation was carried out by using commercially available FDTD software (Lumerical).[46] For simulation, we have selected the silver nanotriangle with an edge length of 120 nm and height of 11 nm surrounded by water (n = 1.333). The refractive index of water decreases monotonically with increasing wavelength from UV to NIR and, in the spectral range considered here, is rigorously described by four-term Sellmeier dispersion formula.[47] Here the dielectric function of water was treated as a constant because the commercial software Lumerical takes into account only non-absorbing and non-dispersive materials as background for physical structures. The *effective* refractive index in the vicinity of the metal surface should be different from that of pure water and can be calculated by integrating the variation of the actual index between the metal

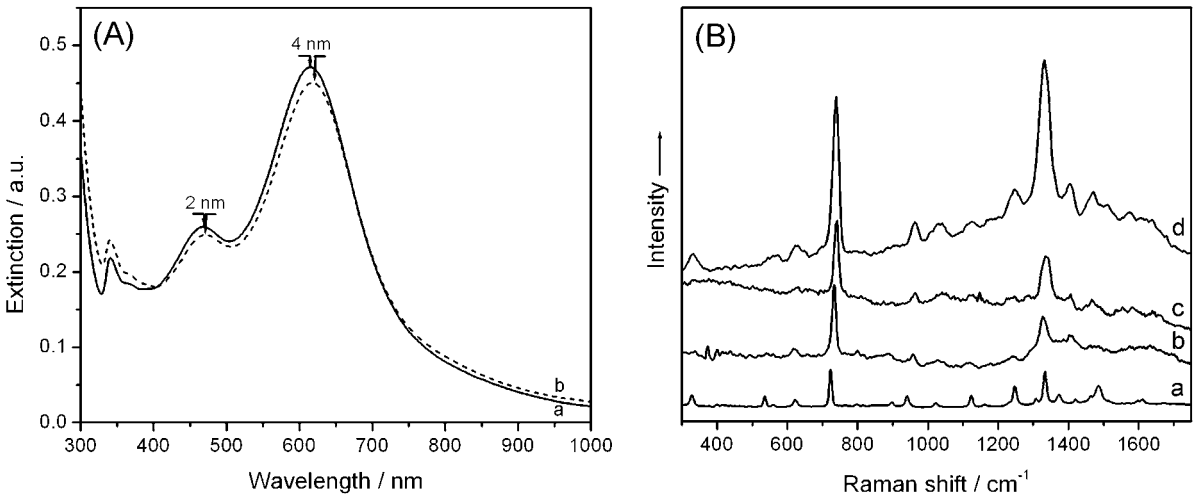

Fig. 7 (A) UV-VIS-NIR extinction spectra of silver colloid (a) before adding adenine and (b) after adding adenine. (B) The normal Raman spectrum of solid adenine (a) and SERS spectra of adenine recorded by laser excitation wavelengths 785 nm (b), 633 nm (c), and 532 nm (d). The final concentration of adenine molecules in the sample solution is 12×10^{-6} M.

surface and the decay length of the electromagnetic field intensity.[48] However, we ignored the chitosan layer because the refractive index of chitosan measured in aqueous solution at similar concentration is in the range of 1.336–1344 close to the water index.[49] The unpolarized laser light at normal incidence to the nanoplate surface was modeled as a superposition of two plane waves linearly polarized along the orthogonal x and z axis. The mesh size used in the FDTD program was 0.5 nm. The Lorentzian expansion of the silver dielectric function used in the simulations was fitted to the experimental data given in literature.[50] Fig. 8 shows the electric field intensity map calculated for the triangular silver nanoplate under excitation at 785 nm, a laser line not far from the main dipolar plasmon resonance (818 nm). The dashed curve in Fig. 1 shows a nice agreement between the experimental and calculated extinction spectra and confirms the previously discussed spectral response of isolated silver nanoplates in the UV-Vis-NIR domain. The dielectric function of silver fitted to the Johnson and Christy published data does not accurately describe the response of silver nanoparticles in the UV because the interband transitions are not taken in consideration.[51] The interband transitions increase the imaginary dielectric function and affect the optical absorption over a range of frequencies including the surface plasmon resonance. The imaginary part of the dielectric function of silver was increased to aid the FDTD code convergence in the UV, which leads to a broader resonance peak at 341 nm and slightly shifted as compared to that from the experiment. This purely numerical adjustment should not affect significantly the plasmon resonances and local field computed in the visible and NIR spectral range, the feature in which we are interested in this work.

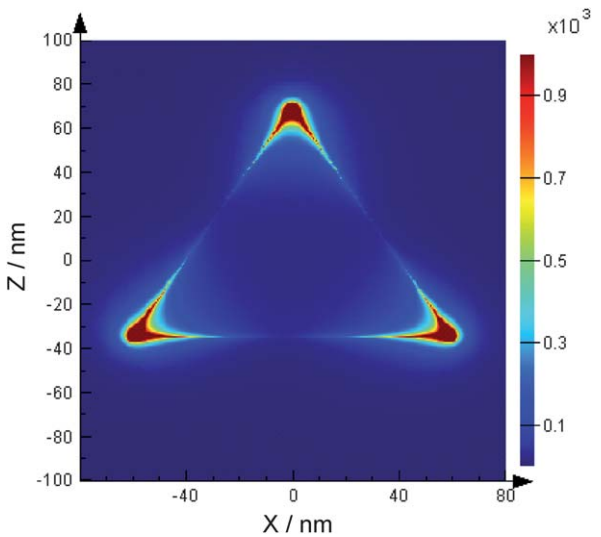

Fig. 8 Calculated $|E|^2$ map for a triangular silver nanoplate of edge length of 120 nm and height of 11 nm under laser excitation at 785 nm, obtained using FDTD simulations.

The computed map in Fig. 8 is in very good agreement with the direct observation of local electromagnetic field for silver triangular nanoparticles (see Fig. 2(b) in ref. 52). Similar simulations were carried out for excitation at 633 and 532 nm laser lines and showed a different pattern of the electric field distribution, involving maxima located at the edges of the triangle in between the corners. According to our simulations, the field intensity has the highest values at the corners, to a lower extent at the edges and less than at the edges and corners, on the faces of the nanoplates. The differences in local field enhancements ($|E_{corner}| > |E_{edge}| > |E_{surface}|$) are in agreement with recently published experimental work which performed SERS imaging on a single gold mesotriangle.[53] In view of our theoretical findings the high SERS activity of chitosan-protected silver nanoplates can be mainly explained by the anisotropy of nanoparticles exhibiting corners and edges which act as individual source of the electromagnetic enhancement. Additional contribution to SERS from the hot-spots located at the nanogaps between some particles, as seen in TEM picture in Fig. 2h, cannot be excluded. Therefore, the amplification of Raman signals as high as 10^6–10^7 in our SERS measurements is fully conceivable by combining the main electromagnetic enhancement of about $(E/E_0)^4 \approx 10^6$ with some contribution from the charge transfer enhancement.[54]

Conclusions

In conclusion, we report the formation of chitosan-coated silver nanoparticles of anisotropic shape, mainly triangular nanoplates, through a seed mediated growth approach. We demonstrate that chitosan plays a multiple role here, from assisting the anisotropic growth to providing high stability and functionality to nanoparticles. The obtained chitosan-coated silver nanoparticles were found to be sensitive LSPR sensors toward the refractive index changes in the surrounding medium and excellent SERS substrates in a wide window of excitation wavelengths, ranging from the visible to near-infrared (NIR). In particular, due to the remarkable stability of chitosan-coated silver nanoparticles, a versatile plasmonic sensor was demonstrated for the first time in solution by combining LSPR and SERS abilities. This LSPR-SERS approach opens a route for multimodal chemical analysis to increase the reliability of biological detection. In particular, as the chitosan provides an excellent, biocompatible shell to silver nanoparticles and exhibits further potential to attach different biological entities, there is significant potential for the use of these nanostructures as multifunctional plasmonic sensors for biodetection of clinically relevant molecules.

Acknowledgements

This work was supported by CNCSIS-UEFISCSU, project number PNII-ID_PCCE_129/2008. The authors are grateful to Dr Lucian Barbu Tudoran for TEM measurements.

References

1 T. Dadosh, J. Sperling, G. W. Bryant, R. Breslow, T. Shegai, M. Dyshel, G. Haran and I. Bar-Joseph, *ACS Nano*, 2009, **3**, 1988–1994.
2 N. I. Cade, T. Ritman-Meer, K. A. Kwakwa and D. Richards, *Nanotechnology*, 2009, **20**, 285201–285206.
3 T. Vo-Dinh, F. Yan and M. B. Wabuyele, *J. Raman Spectrosc.*, 2005, **36**, 640–647.
4 R. Fernandez-Montesinos, P. M. Castillo, R. Klippstein, E. Gonzales-Ray, J. A. Mejias, A. P. Zaderenko and D. Pozo, *Nanomedicine*, 2009, **4**, 919–930.
5 S. Shrivastava, T. Bera, A. Roy, G. Singh, P. Ramachandrarao and D. Dash, *Nanotechnology*, 2007, **18**, 225103–225111.
6 J. L. Elechiguerra, J. L. Burt, J. R. Morones, A. Camacho-Bragado, X. Gao, H. H. Lara and M. J. Yacaman, *J. Nanobiotechnol.*, 2005, **36**, DOI: 10.1186/1477–3155–3–6.
7 B. Pietrobon, M. McEachran and V. Kitaev, *ACS Nano*, 2009, **3**, 21–26.
8 D. M. Ledwith, A. M. Whelan and J. M. Kelly, *J. Mater. Chem.*, 2007, **17**, 2459–2464.
9 Z. Cao, H. Fu, L. Kang, L. Huang, T. Zhai, Y. Maa and J. Yao, *J. Mater. Chem.*, 2008, **18**, 2673–2678.
10 Y. Yang, S. Matsubara, L. Xiong, T. Hayakawa and M. Nogami, *J. Phys. Chem. C*, 2007, **111**, 9095–9104.
11 K. Aslan, J. R. Lakowicz and C. D. Geddes, *Anal. Bioanal. Chem.*, 2005, **382**, 926–933.
12 S. Pal, Y. K. Tak and J. M. Song, *Appl. Environ. Microbiol.*, 2007, **73**, 1712–1720.
13 S. T. Koev, P. H. Dykstra, X. Luo, G. W. Rubloff, W. E. Bentley, G. F. Payne and R. Ghodssi, *Lab Chip*, 2010, **10**, 3026–3042.
14 M. N. V. R. Kumar, R. A. A. Muzzarelli, C. Muzzarelli, H. Sashiwa and A. J. Domb, *Chem. Rev.*, 2004, **104**, 6017–6084.
15 H. Huang and X. Yang, *Biomacromolecules*, 2004, **5**, 2340–2346.
16 M. Potara, D. Maniu and S. Astilean, *Nanotechnology*, 2009, **20**, 315602–315607.
17 D. Wei and W. Qian, *Colloids Surf., B: Biointerfaces*, 2007, **62**, 136.
18 J. N. Anker, W. P. Hall, O. Lyandres, N. C. Shah, J. Zhao and R. P. Van Duyne, *Nat. Mater.*, 2008, **7**, 442–453.
19 V. Canpean and S. Astilean, *Lab Chip*, 2009, **9**, 3574–3579.
20 D. E. Charles, D. Aherne, M. Gara, D. M. Ledwith, Y. K. Gun'ko, J. M. Kelly, W. J. Blau and M. E. Brennan-Fournet, *ACS Nano*, 2010, **4**, 55–64.
21 R. Mehra, *Proc. - Indian Acad. Sci., Chem. Sci.*, 2003, **115**, 147–154.
22 The image processing toolkit Image J is freely available in the public domain at http://rsb.info.nih.gov/ij/.
23 I. Pastoriza-Santos and L. M. Liz-Marzan, *J. Mater. Chem.*, 2008, **18**, 1724–1737.
24 J. E. Millstone, S. J. Hurst, G. S. Metraux, J. I. Cutler and C. A. Mirkin, *Small*, 2009, **5**, 646–664.
25 J. Zeng, Y. Zheng, M. Rycenga, J. Tao, Z.-Y. Li, Q. Zhang, Y. Zhu and Y. Xia, *J. Am. Chem. Soc.*, 2010, **132**, 8552–8553.
26 D. Charles, P. Fournet, S. Cunningham, D. Ledwith, J. M. Kelly, W. Blau and M. E. Brennan-Fournet, *Plasmonics: Metallic Nanostructures and Their Optical Properties VI*, 2008, vol. 7032, p. G322.
27 M. D. Malinsky, K. L. Kelly, G. C. Schatz and R. P. Van Duyne, *J. Phys. Chem. B*, 2001, **105**, 2343–2350.
28 H. Chen, X. Kou, Z. Yang, W. Ni and J. Wang, *Langmuir*, 2008, **24**, 5233–5237.
29 F. Toderas, M. Baia, L. Baia and S. Astilean, *Nanotechnology*, 2007, **18**, 255702–255707.
30 N. Nath and A. Chilkoti, *Anal. Chem.*, 2002, **74**, 504–509.
31 L. J. Sherry, R. Jin, C. A. Mirkin, G. C. Schatz and R. P. Van Duyne, *Nano Lett.*, 2006, **6**, 2060–2065.
32 C. Novo, A. M. Funston, I. Pastoriza-Santos, L. M. Liz-Marzan and P. Mulvaney, *J. Phys. Chem. C*, 2008, **112**, 3–7.
33 P. K. Sudeep, S. T. S. Joseph and K. G. Thomas, *J. Am. Chem. Soc.*, 2005, **127**, 6516–6517.
34 X. Jiang, Q. Zeng and A. Yu, *Langmuir*, 2007, **23**, 2218–2223.
35 L. R. Skewis and B. M. Reinhard, *ACS Appl. Mater. Interfaces*, 2010, **2**, 35–40.
36 X. Zou and S. Dong, *J. Phys. Chem. B*, 2006, **110**, 21545–21550.
37 Z. Sun, C. Wang, J. Yang, B. Zhao and J. R. Lombardi, *J. Phys. Chem. C*, 2008, **112**, 6093–6098.
38 M. Baia, F. Toderas, L. Baia, D. Maniu and S. Astilean, *ChemPhysChem*, 2009, **10**, 1106–1111.
39 D.-Y. Wu, X.-M. Liu, Y.-F. Huang, B. Ren, X. Xu and Z.-Q. Tian, *J. Phys. Chem. C*, 2009, **113**, 18212–18222.
40 Y. Wang, X. Zou, W. Ren, W. Wang and E. Wang, *J. Phys. Chem. C*, 2007, **111**, 3259–3265.
41 A. C. Sant'Ana, T. C. R. Rocha, P. S. Santos, D. Zanchet and M. L. A. Temperini, *J. Raman Spectrosc.*, 2009, **40**, 183–190.
42 X. Qian, X. H. Peng, D. O. Ansari, Q. Yin-Goen, G. Z. Chen, D. M. Shin, L. Yang, A. N. Young, M. D. Wang and S. Nie, *Nat. Biotechnol.*, 2008, **26**, 83–89.
43 L. Rodriguez-Lorenzo, R. A. Alvarez-Puebla, F. J. Garcia de Abajo and L. M. Liz-Marzan, *J. Phys. Chem. C*, 2010, **114**, 7336–7340.
44 B. Giese and D. McNaughton, *J. Phys. Chem. B*, 2002, **106**, 101–112.
45 F. Feng, G. Zhi, H. S. Jia, L. Cheng, Y. T. Tian and X. J. Li, *Nanotechnology*, 2009, **20**, 295501–295506.
46 http://www.lumerical.com/fdtd.php.
47 M. Daimon and A. Masumura, *Appl. Opt.*, 2007, **46**, 3811–3820.
48 C. Yu, L. Varghese and J. Irudayaraj, *Langmuir*, 2007, **23**, 9114–9119.
49 M. Koralewski, K. H. Bodek and K. Marczewsha, *Polish Chitin Society, Monograph XI*, 2006, **XI**, 29–39.
50 H. J. Hagemann, W. Gudat and C. Kunz, *J. Opt. Soc. Am.*, 1975, **65**, 742–744.
51 P. B. Johnson and R. W. Christy, *Phys. Rev. B: Solid State*, 1972, **6**, 4370–4379.
52 J. Nelayah, L. Gu, W. Sigle, C. T. Koch, I. Pastoriza-Santos, L. M. Liz-Marzán and P. A. Van Aken, *Opt. Lett.*, 2009, **34**, 1003–1005.
53 P. R. Sajanlal, C. Subramaniam, P. Sasanpour, B. Rashidian and T. Pradeep, *J. Mater. Chem.*, 2010, **20**, 2108–2113.
54 M. Baia, S. Astilean and T. Iliescu, *Raman and SERS Investigations of Pharmaceuticals*, Springer-Verlag, Berlin, Heidelberg, 2008.